DOI:10.1016/j.jtbi.2014.03.004
Official URL: http://dx.doi.org/10.1016/j.jtbi.2014.03.004

Kinetic modeling in the context of cerebral blood flow quantification by $H_2{}^{15}O$ positron emission tomography: The meaning of the permeability coefficient in Renkin–Crone's model revisited at capillary scale ☆

Sylvie Lorthois [a,b,*], Paul Duru [b,a], Ian Billanou [b,a], Michel Quintard [a,b], Pierre Celsis [c,d]

[a] CNRS, IMFT (Institut de Mécanique des Fluides de Toulouse), Allée Camille Soula, F-31400 Toulouse, France
[b] Université de Toulouse, INPT, UPS, IMFT (Institut de Mécanique des Fluides de Toulouse), Allée Camille Soula, F-31400 Toulouse, France
[c] INSERM, UMR 825, Cerebral Imaging and Neurological Handicaps, Toulouse F-31000, France
[d] Université Toulouse III Paul Sabatier, UMR 825, Toulouse F-31000, France

HIGHLIGHTS

- Fluid dynamic simulations of blood to brain $H_2{}^{15}O$ transfers at capillary scale.
- Renkin–Crone's permeability coefficient is not identical to physiologic permeability.
- Flow rate cannot be determined from micro-scale kinetics by compartmental models.
- An upscaled approach is needed to fully exploit information available from PET.

Keywords:
Brain microcirculation
Numerical simulation
Diffusible tracer
Compartmental approach
Permeability-surface product

ABSTRACT

One the one hand, capillary permeability to water is a well-defined concept in microvascular physiology, and linearly relates the net convective or diffusive mass fluxes (by unit area) to the differences in pressure or concentration, respectively, that drive them through the vessel wall. On the other hand, the permeability coefficient is a central parameter introduced when modeling diffusible tracers transfer from blood vessels to tissue in the framework of compartmental models, in such a way that it is implicitly considered as being identical to the capillary permeability. Despite their simplifying assumptions, such models are at the basis of blood flow quantification by $H_2{}^{15}O$ Positron Emission Tomgraphy.

In the present paper, we use fluid dynamic modeling to compute the transfers of $H_2{}^{15}O$ between the blood and brain parenchyma at capillary scale. The analysis of the so-obtained kinetic data by the Renkin–Crone model, the archetypal compartmental model, demonstrates that, in this framework, the permeability coefficient is highly dependent on both flow rate and capillary radius, contrarily to the central hypothesis of the model which states that it is a physiological constant. Thus, the permeability coefficient in Renkin–Crone's model is not conceptually identical to the physiologic permeability as implicitly stated in the model. If a permeability coefficient is nevertheless arbitrarily chosen in the computed range, the flow rate determined by the Renkin–Crone model can take highly inaccurate quantitative values.

The reasons for this failure of compartmental approaches in the framework of brain blood flow quantification are discussed, highlighting the need for a novel approach enabling to fully exploit the wealth of information available from PET data.

1. Introduction

The methodology commonly used in medical practice to analyze the data obtained from dynamic Positron Emission Tomography (PET) acquisitions is based on kinetic models, which relate the kinetics of the measured radioactive activity and the function under study (Morris et al., 2004). In particular, Cerebral Blood Flow (CBF)

☆**Sources of support requiring acknowledgment:** Région Midi-Pyrénées and Pierre Fabre Dermocosmétique.

* Corresponding author at: CNRS, IMFT (Institut de Mécanique des Fluides de Toulouse), Allée Camille Soula, F-31400 Toulouse, France. Tel.: +33 5 34 32 28 74; fax: +33 5 34 32 29 93.
E-mail address: Sylvie.Lorthois@imft.fr (S. Lorthois).

http://dx.doi.org/10.1016/j.jtbi.2014.03.004

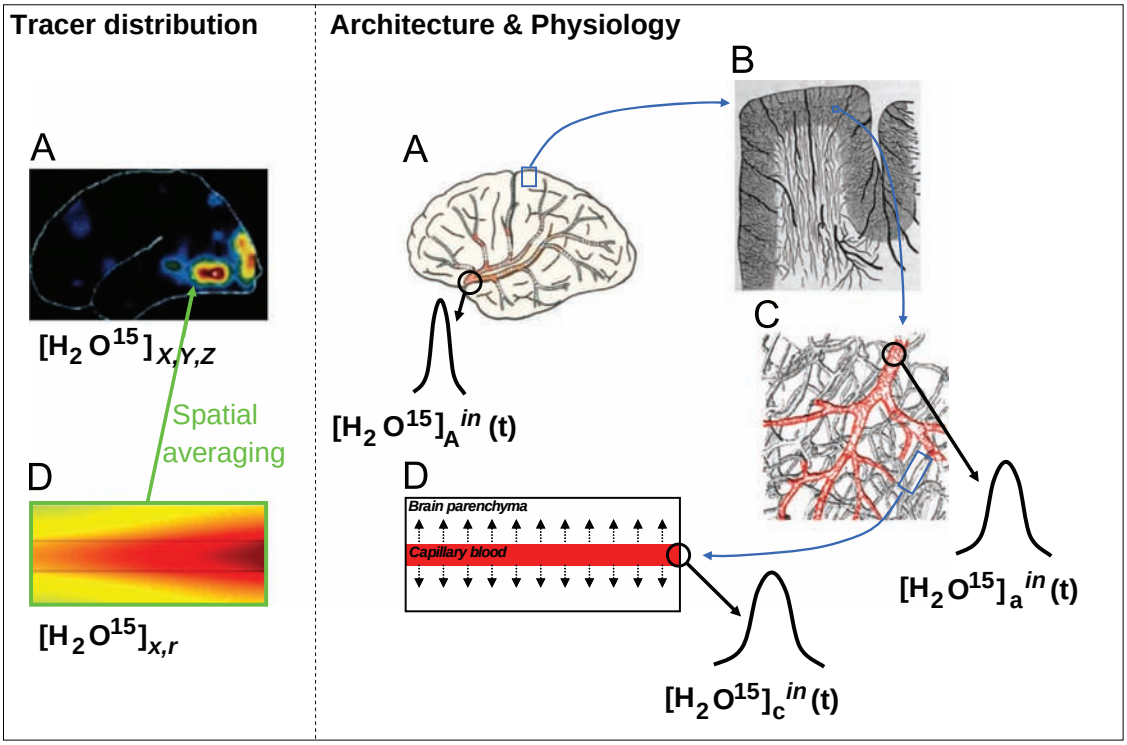

Fig. 1. Schematics of tracer distribution (left) and related phenomena (right) at various relevant scales. A: brain scale; B: macroscopic scale (scale of the cortex); C: mesoscopic scale (scale of the microvacular network: a terminal arteriole is highlighted in red). At this scale, the brain tissue includes both brain parenchyma and the microvascular network; D: microscopic scale (scale of the capillary vessels): at this scale, the extravascular compartment consists in brain parenchyma only. *Left*: typical snapshots of $H_2{}^{15}O$ concentration fields at brain and microscopic scales. *Right*: In addition to the arterial input function $[H_2{}^{15}O]_a^{in}(t)$, the tracer kinetics in brain tissue depends on the architecture of the brain vascular network and on brain physiology. $H_2{}^{15}O$ is indeed transported by the flowing blood, with local flow rates adjusted to the local metabolic needs by neurovascular coupling (see Lorthois et al. (2011a,b) and references therein). In arteries and arterioles, tracer diffusion through the vessel wall can be neglected at first order. Thus, the input function at smaller scales ($[H_2{}^{15}O]_a^{in}(t)$ in arterioles and $[H_2{}^{15}O]_c^{in}(t)$ in capillaries) is essentially delayed and dispersed. Diffusive exchanges between blood and brain parenchyma are preponderant at microscopic scale.

modifications during activation studies are usually determined with the $H_2{}^{15}O$ PET technique, using a kinetic model derived from Kety's and Renkin–Crone's approaches (Kety and Schmidt, 1948; Kety, 1951; Renkin, 1955, 1959; Crone, 1963).

Generally speaking, the concentration of $H_2{}^{15}O$ at a given time in a given brain area depends on three features (see Fig. 1). First, it depends on the time course of the $H_2{}^{15}O$ arterial concentration at brain "inlet" (*arterial input function*); second, on the architecture of the brain vascular network in which $H_2{}^{15}O$ is transported by blood flow; and, third, on brain physiology (including exchange and regulation functions, which determine both CBF and $H_2{}^{15}O$ transfers between blood and brain parenchyma). A kinetic model is a mathematical description relating these three features to the spatiotemporal variations of the concentration of $H_2{}^{15}O$ in the brain, as measured by PET. Its inversion should allow the determination of blood flow from dynamic PET data. Ideally, highly sophisticated models should permit to precisely predict these spatiotemporal variations. However, in practice, a compromise between mathematical complexity, which is imposed by the assumptions made about the vascular architecture and exchange processes, and practical limitations imposed by the measurement technique (spatial and temporal resolution, signal/noise ratio) has to be made (Quarles et al., 1993; St. Lauwrence and Lee, 1998a).

This is why kinetic models such as Kety's and Renkin–Crone's, which combine compartmental concepts with simplified models of perfused capillaries despite incompatible assumptions (see below) have proved to be useful for PET from a practical point of view. However, they exhibits severe limitations, which have been recognized by clinicians and have been put forward to explain some rather contradictory results obtained by PET (Larson et al., 1987; St. Lauwrence and Lee, 1998a,b; Munk et al., 2003a,b). For example, the values of CBF experimentally measured by this approach are lower than the values measured by reference methods, *e.g.*, calculation of CBF from mean transit time using the central volume principle (Raichle et al., 1983) or using radioactive microspheres (St. Lawrence and Lee 1998b), at high flow rates, typically above 40–60 ml/100 g min. Moreover, the measured CBF decreases with increasing acquisition times, which has been named the "falling flow phenomenon" (Raichle et al., 1983; Larson et al., 1987; Walker et al., 2012). Alternately, the standard compartmental parameters, such as the kinetic rate constants in Kety's approach, should be re-interpreted as time-dependent parameters (Munk et al., 2003b, Walker et al., 2012), although they are determined from PET data as constants. These limits, although accepted in the past, become too limitative now that improvements in PET technology have led to scanners with increased sensitivity, which allows for better spatial and temporal resolutions (Munk et al., 2003a, Walker et al., 2012). As a result, some of the current resolving power of PET remains unexploited when analyzing the data using compartmental models (Munk et al., 2003b).

In order to go beyond these limitations, many groups introduced models incorporating additional physiological realism and complexity (Goresky et al., 1970; Larson et al., 1987; Sawada et al., 1989; Bassingthwaighte et al., 1992; St. Lauwrence and Lee, 1998a,b; Munk et al., 2003a,b). However, all these subsequent models have a point in common with the Renkin–Crone approach: the description of the exchange processes between blood and tissue relies on the introduction of a permeability coefficient P (expressed in m/s), which is considered as a physiological constant. This is a crucial point, which enabled Renkin and Crone to introduce ideas derived from microvascular modeling (where tracer concentration varies along the capillaries, *i.e.* a *distributed* approach) in the framework of compartmental approaches (where exchange of tracer takes place between well-mixed compartments with space-independent concentrations).

An implicit assumption is that the permeability coefficient P introduced in Renkin–Crone's and subsequent models is conceptually identical to the physiological capillary permeability to water. The latter is a well-defined concept in microvascular physiology, and linearly relates the net convective or diffusive mass fluxes (by unit area) to the differences in pressure or concentration, respectively, that drive them through the vessel wall (Michel and Curry, 1999).

In this paper, fluid dynamic numerical methods are used to test this assumption. In fact, using computational fluid dynamics, the $H_2{}^{15}O$ transfers between blood and brain parenchyma can be explicitly computed with controlled input parameters (capillary radius, blood volume fraction, flow rate, diffusion coefficients, *etc.*) without the need to introduce any permeability coefficient. By this way, spatially-averaged reference kinetic data, representing the mean $H_2{}^{15}O$ concentration temporal evolution in the tissue (*i.e.* brain parenchyma plus capillary blood, as schematized in Fig. 1), can be obtained at capillary scale, in controlled conditions. Note that such reference kinetic data would be impossible to obtain experimentally from dynamic PET due to its poor spatial resolution and to the need to control and/or measure independently the flow rate at that scale.

Based on such reference kinetic data, the first objective of the present paper is to study whether the permeability coefficient P in Renkin–Crone's model is conceptually identical to the physiological permeability, *i.e.*, independent on other physiological parameters, such as the flow rate. In other word, we want to check whether the analysis of the reference kinetic data by the Renkin–Crone model enables to identify the physiologic capillary permeability. If it happens not to be the case, we want to understand what the intrinsic conceptual limitations of the above compartmental approaches are. The second objective is to discuss the implications of the results obtained at capillary scale, from a theoretical point of view, in the context of blood flow quantification by PET. In particular, we will argue that a novel approach is needed to fully exploit, at a larger scale (voxels or Region of Interests), the wealth of information available from PET data.

2. Background considerations

Several background considerations will first be reviewed. First, the current knowledge about the mechanisms of water exchange through the Blood Brain Barrier (BBB) will be sumarized (Section 2.1). This knowledge indeed constitutes the basis for the choices made for computing the $H_2{}^{15}O$ concentrations at capillary scale in the present paper. Second, the derivation of the Renkin–Crone two-compartment model will be presented, highlighting the underlying assumptions and the rationale for introducing a single permeability coefficient (Section 2.2). The important point here is that these assumptions are much more restrictive than the assumptions used for computing the reference kinetic data, which are finally presented (Section 2.3).

2.1. Mechanisms of water exchange through the BBB

Compared to other organs, the cerebral capillary bed is unique due to the presence of the BBB, the main physiological purpose of which is to keep a constant microenvironment in the cerebral tissue. The BBB is mainly formed by the endothelial cells lining the capillaries, which lack fenestrations and are connected with tight cell–cell junctions (Paulson, 2002; Hawkins and Davis, 2005). Compared to the discontinuous or fenestrated capillaries found in other organs, these tight junctions restrict the paracellular transfers of water and solutes across the BBB. Despite this restriction, the distribution of labeled water directly injected into the cerebrospinal fluid and diffusing through the brain parenchyma is dominated by loss across capillary walls and subsequent removal into the blood flow by moving across the BBB (Fenstermacher and Kaye, 1988; Nicholson, 2001), with efflux half-time of $\sim$1.5 min. Water can indeed pass through endothelial cells by several passively driven diffusive mechanisms (Kimelberg, 2004): diffusion through the phospholipid bilayer, a relatively slow process (Papahadjopulos and Kimelberg, 1974; Agre et al., 2004; Heymann and Engels, 1999), cotransport with organic or inorganic ions (MacAulay et al., 2004) and, possibly, facilitated diffusion through specialized water channels (Amiry-Moghaddam et al., 2004; Dolman et al., 2005). In the present study, the transfer of $H_2{}^{15}O$ to the tissue through the BBB will thus be modeled as being purely diffusive as in Renkin–Crone's approach. These transfers will be characterized by an effective diffusion coefficient, the value of which is justified in Section 3, without any *a priori* assumption regarding the value of the physiologic capillary permeability.

2.2. Derivation of the Renkin–Crone two-compartment model

Independently on these considerations at molecular scale, the first kinetic models used for CBF quantification were based on empirical observations using various diffusible tracers at larger scale, *i.e.*, whole brain scale, for which the washout curves are approximately mono-exponential (Lassen and Perl, 1979). The very first one is a two compartmental model, proposed by Kety and Schmidt (1948). In such models, an arterial compartment and a tissue compartment (including the brain parenchyma as well as the microvascular network) are considered. The tracer is assumed to be homogeneously distributed in each compartment (well-mixed compartments) and exchanges between these two compartments are described using a first-order kinetic law, leading to:

$$\frac{dC_t(t)}{dt} = k_1 C_a(t) - k_2 C_t(t), \tag{1}$$

where C_a and C_t are the (homogeneous) concentration of $H_2{}^{15}O$, expressed in mol/m^3, in the arterial and tissue compartments, respectively, and k_1 and k_2 are two kinetic rate constants, expressed in s^{-1}. Here, note that, for clarity, SI units are used contrarily to what is usually done in PET kinetic modeling (in the context of blood flow rate quantification), where

- a distinction is often made between the unit for volume of blood (ml) and the unit for volume of tissue (cm^3), leading for different units for k_1 and k_2 (Innis et al., 2007) and
- a normalization by a given mass or volume of brain tissue (typically 100 g or 100 ml) is often performed.

Eq. (1) typically represents the exchange between two phases with a local thermodynamic equilibrium at the interface and different affinities of the tracer for both phases. Consequently, there is a difference in the equilibrium $H_2{}^{15}O$ concentrations in each compartment characterized by a partition coefficient λ_d equals to k_1/k_2. For a given evolution of concentration in the arterial compartment, the solution of Eq. (1) is (with $C_t(t=0)=0$):

$$C_t(t) = k_1 C_a(t) \otimes e^{-(k_1/\lambda_d)t}, \tag{2}$$

where the symbol $\otimes$ denotes the time convolution product over the time interval $[0, t]$. If the arterial concentration at brain inlet is known (either using arterial catheterization, which has major constraints for both patient and practitioner or alternative atraumatic techniques such as direct determination from dynamic PET brain images or external monitoring of the pulmonary concentration), the rate

constant k_1 can be deduced by minimizing the difference between $C_t(t)$ as predicted by Eq. (2) and $C_t(t)$ as measured by PET. From this point, the major difficulty is to relate the constant k_1 to CBF, especially in the perspective of local CBF quantification.

In the case of global CBF quantification, which was the focus of Kety's approach, mass conservation over the whole brain volume written during the first pass of the tracer leads to (Morris et al., 2004):

$$k_1 = \frac{QE}{v}, \tag{3}$$

Q being the CBF expressed in m^3/s, v being the volume of brain tissue, which, in Kety's approach, is defined as *including its contained blood*, and E being the extraction coefficient, *i.e.*, the proportion $(C_a - C_v)/C_a$ of tracer extracted between brain arterial inlets and venular outlets. Thus, determining CBF by Kety's approach requires additional knowledge of the venous concentration C_v.

In order to progress toward local CBF quantification and to avoid additional venous sampling, Kety (1951) and, subsequently, Renkin and Crone (Renkin, 1955, 1959; Crone, 1963) aimed at expressing the extraction coefficient as a function of other physiological parameters that could be determined independently. For that purpose, based on the ideas proposed by August Krogh to describe oxygen transfers in skeletal muscles (Krogh, 1919), they modeled the diffusive exchanges between one single cylindrical capillary vessel and its immediate surrounding tissue unit, isolated from other capillaries (Fig. 2). They argued that, during its single path through the capillary, the tracer diffuses towards a large, well-mixed extravascular space, where its concentration remains close to zero due to dilution. Accounting for longitudinal variations of tracer concentration in the vessel, which had been previously neglected by Kety, but still neglecting the contribution of the intravascular tracer to the measured concentration, their major result was the following expression:

$$E = 1 - e^{-PS/Q}, \tag{4}$$

relating the extraction coefficient E to the flow rate Q in the vessel and to its *permeability-surface product*, *i.e.*, the product of a permeability coefficient P (expressed in m/s), considered as a physiological constant, and of the surface S of the vessel wall (Fig. 2). Here, the description of the exchange processes between blood and tissue is a crucial point in the modeling. Consistent with the knowledge on the mechanisms of water exchange through the BBB at molecular scale, the transfer of $H_2{}^{15}O$ between the arterial and tissue compartments is assumed to be purely diffusive. The diffusive flux is obtained by writing the steady-state solution of Fick's diffusion law across a membrane of given thickness τ separating the two tracer reservoirs of constant concentration. This assumption is often referred to as an "adiabatic" assumption, meaning that the rates of variation of the tracer concentration in each compartment are much slower than diffusion across the membrane so that the resulting diffusive flux can be obtained using the classical steady state solution (Lassen and Perl, 1979). Moreover, the concentration of $H_2{}^{15}O$ in the capillary vessel, $C_c(x,t)$, is supposed to only depend on the longitudinal position x in the capillary. The concentration in the tissue, C_t, is assumed to be homogeneous.

Based upon these assumptions, the diffusive surface flux can be written as

$$J(x,t) = -P(C_c(x) - C_t(t)/\lambda_d), \tag{5}$$

where, considering a unit partition coefficient of the tracer between the membrane medium, *i.e.*, the endothelial layer, and blood, the membrane permeability P is given by the following relationship (Lassen and Perl, 1979):

$$P = D/\tau, \tag{6}$$

where D is the effective diffusion coefficient of the tracer in the membrane of thickness τ.

2.3. Current approach: insight from numerical simulation

By contrast, in the computational approach used for calculating the reference kinetic data in the present work, the diffusive fluxes between blood and tissue across the BBB are written by using Fick's diffusion law (see Section 3, Eq. (8)), *i.e.* without introducing any permeability coefficient, the use of which is not even required when writing the model equations (see Section 3.1). Therefore, while keeping the original assumptions of Renkin and Crone regarding the vascular architecture, *i.e.*, Krogh cylinder (Fig. 2), and exchange processes through the endothelial layer, *i.e.*, pure diffusion, no additional assumption, such as the adiabatic approximation and/or assumptions about the mixing of the tracer in a given compartment is made. By this way, the full spatiotemporal complexity of the problem is considered, including transient states. Moreover, in this computational framework, additional geometric complexity can be introduced, by explicitly adding a third phase of reduced diffusion coefficient representing the endothelial layer (see Fig. 2 and Section 3 for details). This allows the influence of the Blood Brain Barrier to be quantitatively studied.

3. Materials and methods

3.1. Reference kinetic data: numerical simulations

Transfers between blood and tissue at capillary scale in the Krogh cylinder axi-symmetric geometry (see Fig. 2) are computed

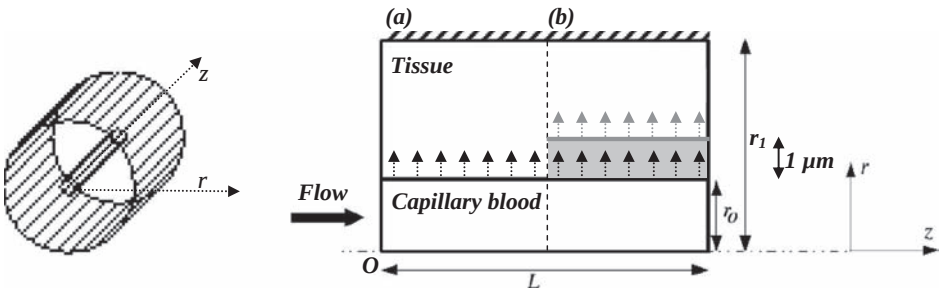

Fig. 2. Krogh cylinder geometry (not to scale) and notations used for the numerical simulations. *Left:* three-dimensional representation, highlighting a unique capillary surrounded by an isolated tissue cylinder; *Right:* two-dimensional representation of half the computational domain in the *Orz* plane. The whole computational domain is constructed by symmetry of revolution around the *Oz* axis. The total flux at the capillary/tissue interface is given by SJ, where S is the area of this interface ($2\pi r_0 L$) and J is the surface flux, represented by individual arrows. (a) Classical Krogh cylinder geometry. (b) Variant including a third phase representing the endothelial layer (schematized in gray).

Table 1
Numerical values or ranges of the parameters used for numerical simulations. When possible, these values have been taken from the literature (see references indicated by the first letters of the author's name and publication year) or calculated from literature values.

	Numerical values	Refs.		Numerical values	Refs.
Capillary radius (r_0)	2–4.5 μm	Cas06	Diffusion coefficient of $H_2{}^{15}O$ in whole blood (D_b)	2×10^{-9} m²/s	Sta98
Capillary length (L)	60 μm	Cas06	Diffusion coefficient of $H_2{}^{15}O$ in tissue (gray matter) (D_t)	0.75×10^{-9} m²/s	Tho00
Blood volume fraction (ν_c/ν)	2%	Cas06	Diffusion coefficient of $H_2{}^{15}O$ through the endothelium (D_e)	$D_b/100$–D_t	Cal83, Rud04, Hey99
Krogh cylinder radius ($r_1 = r_0\sqrt{\nu/\nu_c}$)	14–32 μm		Flow rate	5×10^{-3}–3.3 nl/s	Lor11a
Capillary wall thickness (τ)	1 μm	Coo87 Par02	Concentration of tracer solution (C_{max})	0.02 mol/m³	
Partition coefficient (λ_d)	1 g/g (gray matter) 0.95 g/g (whole brain)	Her85	Beginning of injection (t_0) End of injection (t_1)	2 s 15 s	
$H_2{}^{15}O$ radioactive decay (κ)	0.0058/s	Ame08	Smoothing coefficient δt	0.5 s	

by solving a convection-diffusion equation in the blood domain, where the velocity profile is assumed to be parabolic (Poiseuille's law) and independent of time, and a diffusion equation in the tissue domain. In practice, we write

$$\frac{\partial C_\alpha}{\partial t} + \mathrm{v}_\alpha \cdot \nabla C_\alpha = \nabla \cdot (D_\alpha \nabla C_\alpha) - \kappa C_\alpha, \tag{7}$$

where α indexes either phases (capillary blood ($\alpha = c$) or tissue ($\alpha = t$)), κ is the radioactive extinction coefficient of $H_2{}^{15}O$, D is the effective diffusion coefficient and $\boldsymbol{v}$ the local velocity ($\boldsymbol{v}_c = 2Q/\pi r_0{}^2(1-(r^2/r_0{}^2)) \cdot e_x$ in the capillary vessel, where r is the radial coordinate, and $\boldsymbol{v}_t \equiv 0$ in the tissue).[1]

Following Renkin and Crone, the exchange processes between blood and tissue are assumed to be purely diffusive, and the most simple and general forms of corresponding boundary conditions at the vessel wall ($r = r_0$) are used. The first boundary condition corresponds to the continuity of fluxes (Nicholson, 2001):

$$J(x,t) = -D_c \left.\frac{\partial C_c}{\partial r}\right|_{r=r_0{}^-} = -D_t \left.\frac{\partial C_t}{\partial r}\right|_{r=r_0{}^+}, \tag{8}$$

assuming that there is no tracer accumulation nor loss at the vessel wall. The second boundary condition

$$C_c|_{r=r_0{}^-} = \lambda_d \, C_t|_{r=r_0+}, \tag{9}$$

expresses the local thermodynamic equilibrium at the interface, which leads to a concentration discontinuity due to the difference of affinity of the tracer for blood and tissue.

At the capillary inlet ($x = 0$), the time-course of tracer concentration is imposed by a smoothed Heaviside function

$$C_c(0,r,t) = C_a(t) = \begin{vmatrix} 0, & 0 \le t \le t_0 - \delta t \\ smoothed, & t_0 - \delta t < t < t_0 + \delta t \\ C_{max}, & t_0 + \delta t \le t \le t_1 - \delta t \\ smoothed, & t_1 - \delta t < t < t_1 + \delta t \\ 0, & t_1 + \delta t \le t \end{vmatrix} \tag{10}$$

where t_0 and t_1 represent the beginning and end of injection and δt is a smoothing parameter.[2]

At the capillary outlet ($x = L$), a free convection boundary condition is used,[3] *i.e.*

$$\left.\frac{\partial C_c}{\partial x}\right|_{x=L} = 0, \tag{11}$$

in the expression of the total flux.

The tissue cylinder is isolated, leading to zero fluxes at its proximal and distal ends:

$$\left.\frac{\partial C_t}{\partial x}\right|_{x=0,L} = 0, \tag{12}$$

and at its exterior boundary ($r = r_1$)

$$\left.\frac{\partial C_t}{\partial r}\right|_{r=r_1} = 0. \tag{13}$$

These equations are implemented using the finite-element commercial software Comsol Multiphysics®. This software allows computing the temporal evolution of the concentration field in the considered geometry as a function of an imposed set of entry parameters. The numerical values of these parameters, which altogether define the idealized architecture, physiology and dynamics of the tracer injection, are displayed in Table 1 and discussed at the end of the present section. The reference kinetic data are subsequently evaluated, at each time step, by integrating over the whole geometry (*i.e.*, without neglecting the vascular contribution of $H_2{}^{15}O$ to the signal):

$$C_{ref}(t) = \frac{1}{\nu}\int_{\nu_c} C_c(t)\, d\nu_c + \frac{1}{\nu}\int_{\nu_t} C_t(t)\, d\nu_t. \tag{14}$$

Note that, in order to evaluate the influence of reduced water diffusion through the brain capillaries endothelium, additional simulations have been performed by explicitly adding a third phase ($\alpha = e$) of reduced diffusion coefficient and of 1 μm thickness, representing the endothelial layer between blood and tissue ($r_0 < r < r_0 + 1$ μm). In this case, additional equations are introduced along the same line as above. Eq. (7) still holds in the endothelial phase, where the local convective velocity $\boldsymbol{v}_e$ is null. Replacing subscript t by subscript e in Eq. (11) yields a new equation representing null fluxes at the proximal and distal ends of the endothelial layer. The same replacement is performed in Eq. (8). Along with the assumption of tracer concentration continuity at the blood/endothelium interface (partition coefficient equals to one), these two equations represent the boundary conditions for

[1] Here, we assume that the concentration of $H_2{}^{15}O$ is small enough so that the total density is constant and, as a consequence, Eq. (7) is also valid when concentrations are expressed in mol/m³. In addition, the diffusive flux in this tracer case is written under the form of a simple Fick's law (Taylor and Krishna, 1993).

[2] In practice, this input function is implemented using the flc2hs MATLAB function, a smoothed Heaviside function with a continuous second derivative without overshoot, defined by a sixth-degree polynomial.

[3] It must be reminded that this boundary condition works well, *i.e.*, is physically representative, if the Péclet number for the flow in the vessel ($Pe = LQ/(\pi r_0^2 D_b)$), calculated with the vessel length, is larger than one, which is always the case in this study, where Pe is between 1.7 and 9000.

diffusive exchange between blood and endothelium. Finally, the equations representing the boundary conditions between endothelium and tissue are the following:

$$J(x,t) = -D_e \frac{\partial C_e}{\partial r}\bigg|_{r=1+r_0^-} = -D_t \frac{\partial C_t}{\partial r}\bigg|_{r=1+r_0^+}, \tag{15}$$

and

$$C_e|_{r=1+r_0^-} = \lambda_d \, C_t|_{r=1+r_0^+}. \tag{16}$$

After numerically solving this new set of equations, the reference kinetic data $C_{ref}(t)$ are evaluated as above by integrating the obtained concentration field over the whole geometry. Note that if D_e equals the effective diffusion coefficient in brain tissue, the situation reduces to the previous Krogh cylinder geometry with only two phases.

3.2. Identification of the permeability coefficient

Contrary to real PET experiments where the flow rate at capillary scale is unknown, this parameter is imposed in the above numerical approach. The knowledge of the flow rate can thus be used to identify the permeability coefficient from the computed reference kinetic data. For that purpose, the single adjustable parameter in Eq. (2), k_1, is numerically determined by minimizing the difference between the reference kinetic data $C_{ref}(t)$ and $C_t(t)$, *i.e.*, minimizing the following norm $N(k_1)$:

$$N(k_1) = \left| C_{ref}(t) - k_1 C_a(t) \otimes e^{-(k_1/\lambda_d)t} \right|^2, \tag{17}$$

using a data fitting algorithm in least-squares sense (Matlab function "lsqcurvefit").

Combining Eqs. (3) and (4) leads to

$$k_1 = \frac{Q}{v}\left[1 - e^{-PS/Q}\right]. \tag{18}$$

As the flow rate, the capillary surface and the total volume are known parameters used as inputs for the numerical simulations, the permeability coefficient is subsequently determined from k_1 by

$$P = -\frac{Q}{S}\ln\left[1 - \frac{k_1 v}{Q}\right], \tag{19}$$

provided that $k_1 v/Q < 1$. Otherwise, P cannot be determined and, as a consequence, has no physical meaning.

3.3. Identification of the flow rate

Alternatively, if the flow rate is considered as unknown, but with known permeability coefficient, capillary surface and total volume, the flow rate can be determined from k_1, provided that $PS > k_1 v$, by inversing Eq. (18):

$$Q = \frac{k_1 v \, PS}{k_1 v \, LambertW[-(PS/k_1 v)\exp(-(PS/k_1 v))] + PS}, \tag{20}$$

where *Lambert W* is Lambert's *W* function (Weisstein, 2002).

3.4. Reference physiological data used in numerical simulations

In this section, the values of the physiological parameters used in the numerical study (see Table 1) are briefly justified, when necessary.

First, the effective coefficient of diffusion of $H_2{}^{15}O$ through the capillary endothelium depends on the relative contribution of the passive diffusive mechanisms involved at molecular scale (see Section 1), which is still unknown (Kimelberg, 2004). However, in physiological conditions, fine systemic osmoregulation (Bourque, 2008) ensures that the brain interstitial fluid is in osmotic equilibrium with the blood plasma (Boulard, 2001; Maallem et al., 2006), which nullifies the contribution of osmotic forces. The relative contribution of trans- and paracellular pathways also remains controversial. Several authors note that the transcellular contribution should be small (Michel and Curry, 1999; Li et al., 2010) when others note that it should be preponderant (Fraser and Dallas, 1990) because the tight junctions prevent bulk (convective) paracellular flow of water and solutes (Paulson et al., 1977; Go et al., 1981; Paulson, 2002) and even restrict paracellular diffusion (Hawkins and Davis, 2005).

Clearly, a lower bound value for D_e is given by the diffusion coefficient across lipid bilayers (~ 0.5–0.7×10^{-10} m^2/s) (Callaghan et al., 1983; Rudakova et al., 2004), *i.e.*, close to one hundredth of the diffusion coefficient of water in whole blood ($D_s = 2 \times 10^{-9}$ m^2/s, Stanisz et al., 1998). An upper bound value corresponds to the diffusion coefficient in brain tissue ($D_t = 0.75 \times 10^{-9}$ m^2/s, Thomas et al., 2000). Therefore, in order to evaluate the influence of reduced water diffusion through the brain capillaries endothelium, the effective diffusion coefficient through the endothelial cells, D_e, has been varied between 0.2×10^{-10} m^2/s and the value of the effective diffusion coefficient in brain tissue, see Table 1. In the latter case, the situation reduces to the Krogh cylinder geometry with only two phases. Moreover, the blood/tissue partition coefficient λ_d, expressed in g/g, has been varied from 0.95 (whole brain) to 1 (gray matter) (Herscovitch and Raichle, 1985).

Second, even if the human brain capillary mesh is architecturally much more complex (Cassot et al., 2006; Lauwers et al., 2008) than a bundle of parallel Krogh cylinders, it has been recently demonstrated that it becomes homogeneous and space-filling over a cut-off length corresponding to the characteristic capillary length, typically 60 μm (Lorthois and Cassot, 2010; Cassot et al., 2006). On average, no point in the tissue compartment is further away from some point of the vasculature than half of this characteristic length. On smaller length scales, brain capillary diameters are distributed and range from ~ 4 to ~ 9 μm. Geometrical parameters displayed in Table 1 have been chosen accordingly, the radius of the effective extravascular Krogh cylinder being calculated in order to match the known value of the brain microvascular density ($\sim 2\%$) and the thickness of capillary wall being fixed to 1 μm, *i.e.*, an intermediate value when compared to data from the literature (Pardrige, 2002, Coomber et al., 1987).

Third, the significant heterogeneity in brain capillary diameters and network connectivity is known to induce large heterogeneities of blood flow (Pawlik et al., 1981; Kuschinsky and Paulson, 1992; Villringer et al., 1994), which span several orders of magnitude in capillaries of given diameter (Lorthois et al., 2011a). Therefore, in the present work, the flow rate in the capillary vessel has been varied from 5×10^{-3} nl/s (0.3 nl/min) to 3.3 nl/s (200 nl/min).

Finally, the tracer bolus at capillary inlet is modeled using a smoothed Heaviside function (Eq. (10)). Its time span ($t_1 - t_0$) has been fixed to 13 s, according to the clinical protocol for $H_2{}^{15}O$ injection at the PET Center, University Hospital Purpan, Toulouse and its concentration has been chosen arbitrarily.

Note that due to delay and dispersion, the signal after some travel distance will feature lower frequencies. Several relaxation times indeed characterize the physics of the increasing and then decreasing concentration in the Krogh cylinder:

- since the Péclet number is relatively large in the capillary domain, we are mainly interested in the advection travel time, which will change here with velocity,
- diffusion relaxation times play essentially a significant role in the tissue domain. This point is discussed below.

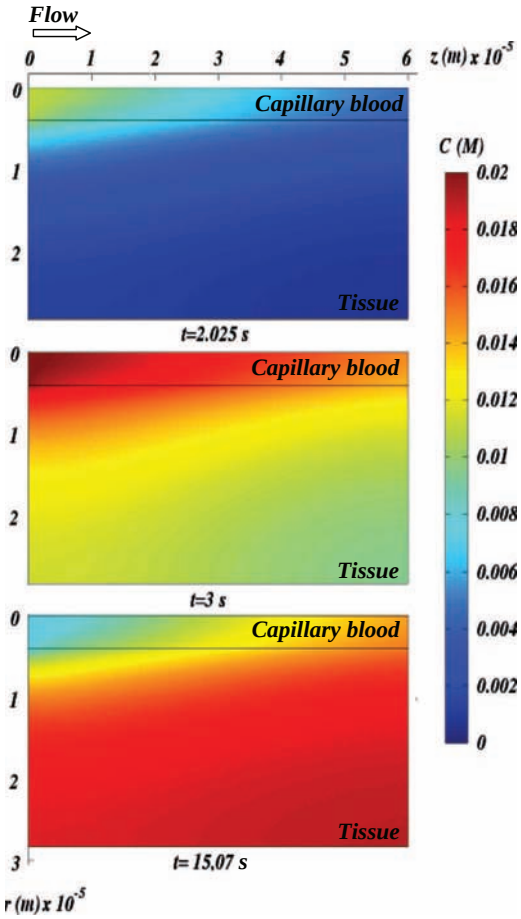

Fig. 3. Numerical simulations: transient concentration fields in the classical Krogh cylinder geometry. $H_2{}^{15}O$ concentration field calculated by numerical simulations in a 4 μm radius capillary tube with blood flowing at 11.31 nl/min (λ_d=1). Tracer spatial repartition at the very beginning of injection ($t=t_0+0.025$ s, top panel), after one second of infusion ($t=t_0+1$ s, middle panel) and at the very beginning of clearance ($t=t_1+0.07$ s, bottom panel).

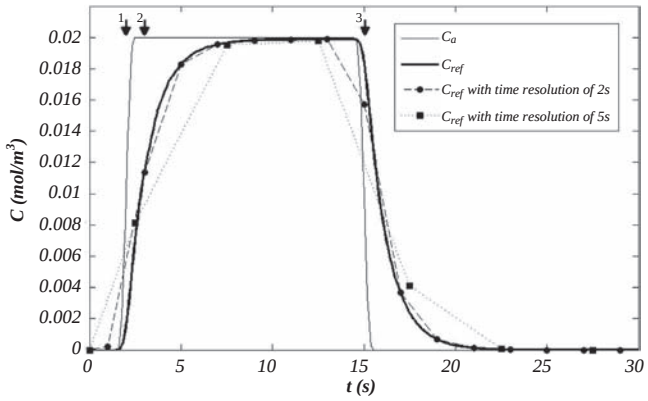

Fig. 4. Numerical simulations: tracer kinetics corresponding to the mean concentration fields displayed on Fig. 3, for various time resolutions of the PET camera. Bold line: no limitation on time resolution; dashed line: time resolution of 2 s; dotted line: time resolution of 5 s. The input function is superimposed on the same figure (plain line). Arrows highlight the times corresponding to the three snapshots displayed in Fig. 3, *i.e.* the beginning of injection (Arrow 1; $t=t_0+0.025$ s), the time after 1 s of infusion (Arrow 2; $t=t_0+1$s), and the beginning of clearance (Arrow 3; $t=t_1+0.07$ s).

First, it is important to recognize that the buildup of concentration in the tissue domain, once the concentration C_c has been changed, will depend mathematically on the spectrum of eigenvalues of the diffusion operator over the tissue geometry, as it may be inferred from a discussion of a similar problem in a different context (Landereau et al., 2001). Typically, the real response of the system will involve a convolution with a series of exponentials, each exponential having a characteristic time determined by one of the eigenvalues. A step function is a good test of the response of the system since it involves the whole frequency spectrum.

Second, the time span (t_1-t_0) will have to be compared with the relaxation time for the tissue domain to reach so-called equilibrium. If (t_1-t_0) is lower than this relaxation time, the maximum averaged concentration in the tissue will be lower than the maximum of the imposed concentration multiplied by the partition coefficient. This interesting feature of the system's behavior is easily observed using the chosen inlet condition (see Golfier et al. (2007) for an example of such a discussion in a mathematically similar but different context).

Therefore, since this paper is focused on understanding the conceptual limitations of the Renkin–Crone approach at capillary scale, which might appear whatever the particular shape of the input function, the chosen inlet condition represents the most challenging choice.

4. Results and discussion

4.1. Reference kinetic data: numerical simulations and resulting insights on capillary-tissue exchange

Typical snapshots of the $H_2{}^{15}O$ concentration field in the Krogh cylinder at the beginning of injection ($t=t_0+0.025$ s), after 1 s of infusion ($t=t_0+1$ s) and at the beginning of clearance ($t=t_1+0.07$ s), are presented in Fig. 3. From these concentration fields, the mean concentration of $H_2{}^{15}O$ in the whole domain is computed at each time step using Eq. (14) to obtain the reference kinetic data $C_{ref}(t)$ (see Fig. 4, bold line). This reference kinetic data represents what would be acquired using a perfect PET camera, *i.e.* with no limitation on spatial and temporal resolution, no noise, and a perfect reconstruction algorithm, while typical dynamic PET time scales are two to five seconds (see Fig. 4, dashed and dotted lines, respectively), at best. This limitation on temporal resolution produces a smoothing of the kinetic data, especially when input variations are quick, such as at the beginning of injection (Arrow 1) and clearance (Arrow 3). This smoothing effect is neglected in the whole following.

Influence of geometry (capillary radius), flow rate, reduced water diffusion through the brain capillaries endothelium and partition coefficient is displayed on Fig. 5. In all cases, as expected, the mean concentration increases during the injection phase and starts to decrease when injection stops. For a given geometry, the dynamics of C_{ref} in both phases is more rapid when the flow rate increases (filled *vs.* corresponding empty symbols in Fig. 5a and b). Moreover, for a given flow rate, it is more rapid when the capillary radius decreases (squares *vs.* circles in Fig. 5a and b). In both cases, reducing the effective diffusion coefficient in the capillary wall (Fig. 5b *vs.* a) slows down the response of the system, while reducing the partition coefficient reduces the maximal concentration. Thus, in the whole following, the results will be presented as a function of radius and flow rate for the two extreme cases: the most rapid ($\lambda=1$, $D_e=D_t$) and the slowest ($\lambda=0.95$, $D_e=D_s/100$) ones.

In all cases, equilibrium between blood and tissue, where concentration gradients in both compartments as well as diffusive transfers through the vessel wall are null, is reached for the largest flow rates investigated: C_{ref} then reaches $C_{eq}=C_{max}(d_v+\lambda_d(1-d_v))$ (see, *e.g.*, filled symbols in Fig. 5a). Indeed, when the flow rate is above a threshold and the duration of the input function plateau is

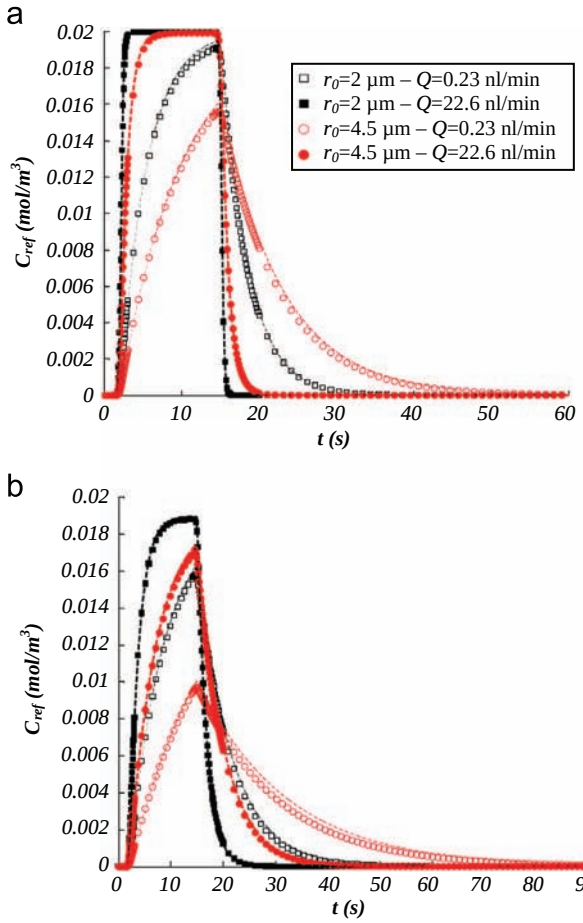

Fig. 5. Numerical simulations: tracer kinetics. Mean concentration of $H_2{}^{15}O$ in the whole computational domain as a function of time. Results are shown for four combinations of two flow rates (0.23 nl/min and 22.62 nl/min) and two radii (2 µm and 4.5 µm). (a) $D_e=D_t$, $\lambda_d=1$. (b) $D_e=D_s/100$, $\lambda_d=0.95$. Symbols: results obtained by numerical simulations. Dashed lines: best fits of the numerical results by Eq. (2) (Pearson's r correlation coefficient is typically greater than 0.98). See inserted legends for details.

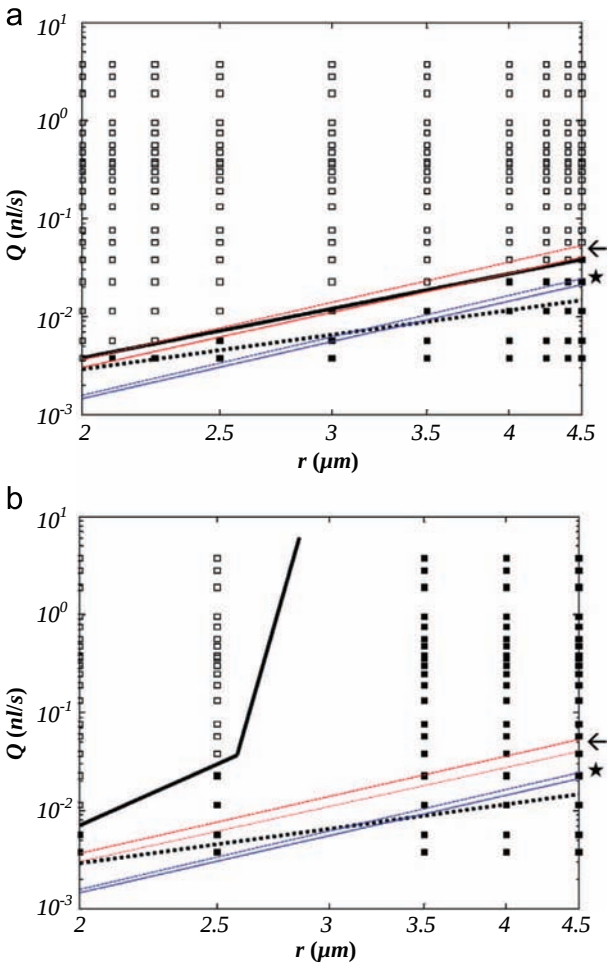

Fig. 6. Numerical simulations: tracer exchange regime maps. (a) $D_e=D_t$, $\lambda_d=1$. (b) $D_e=D_s/100$, $\lambda_d=0.95$. Open squares indicates simulations for which the mean $H_2{}^{15}O$ concentration reaches a value higher than 99.5% of the equilibrium concentration C_{eq}, *i.e.* equilibrium is reached during tracer injection. Filled squares indicate simulations for which equilibrium is not reached. The transition between these two regimes is shown as a bold solid line and can be fitted by a power law $Q_{threshold}=Kr_0{}^{\gamma}$ in (a). Bold dotted line: transition in case of instantaneous diffusion. Thin lines: flow rate *vs.* capillary radius relationship from Lorthois et al., 2011a,b, without (continuous) or with (dotted) 25% vasodilatation, with low BC (blue, highlighted by stars) or high BC (red, highlighted by arrows).

larger than the characteristic time for diffusion in the tissue domain, the total supply of tracer is sufficient for the system to reach equilibrium before rinsing.

At capillary scale, the diffusion distance traveled within the tissue compartment by the tracer during injection ($\sqrt{D_t(t_1-t_0)}$=987 µm) is always larger than the radius of the tissue cylinder (see Table 1), demonstrating that the limiting phenomenon for reaching equilibrium is convection. Thus, a lower-bound value for this flow rate threshold can be calculated, assuming that diffusive transfers are instantaneous, neglecting backdiffusion and the convective tracer clearance. In this case, the total amount of injected tracer ($QC_{max}(t_1-t_0)$) remains in the system, the mean concentration of which being therefore $d_vQC_{max}(t_1-t_0)/\pi Lr_0^2$, where d_v is the blood volume fraction ($d_v=v_c/v$). This mean concentration reaches the equilibrium concentration C_{eq} as soon as the flow rate is above $\pi Lr_0^2/(d_v+\lambda_d(1-d_v))d_v(t_1-t_0)$. The real threshold is greater than this theoretical value and can be estimated by seeking the flow rate for which the maximal value of $C_{ref}(t)$ reaches 99.5% of C_{eq}.

Fig. 6 shows two typical tracer exchange regime maps, for the two extremes cases defined above. For all the cases investigated in the present study (presence of an endothelial layer reducing the diffusion coefficient or not, partition coefficient between blood and tissue taken into account or equal to 1), except one ($\lambda_d=0.95$, $D_e=D_s/100$) where the equilibrium is not reached for the highest

Table 2
Best fit for coefficients of power law $Q_{threshold}=Kr_0^{\gamma}$, as a function of the reduced diffusion in the endothelial layer (NE: no endothelial layer) and of the partition coefficient. r_0 must be expressed in micrometers for a flow rate expressed in nl/s.

Parameters		***Results***	
λ	D_e (10^{-9} m^2/s)	log(K)	γ
1	0.75 (NE)	−3.28	2.85
1	0.4	−3.2841	2.9828
1	0.2	−3.2841	2.9828
0.95	0.4	−3.22	2.68
0.95	0.2	−3.18	2.74
0.95	0.02	–	–

radii (see Fig. 6b), the flow rate threshold value can be related to the capillary radius by a power law ($Q_{threshold}=Kr_0{}^{\gamma}$), with a scaling exponent γ between 2.2 and 3.16 depending on the magnitude of reduced water diffusion through the brain capillaries endothelium (see Fig. 6a, bold continuous lines, and Table 2).

These values found for $Q_{threshold}$ can be compared to the hemodynamic conditions prevailing in capillaries, in order to

assess the regime of tracer exchange in the human brain microcirculation. Despite large heterogeneities of flow rates in these vessels, numerical simulations of blood flow in anatomically accurate large human vascular networks have demonstrated that the mean value of the flow rate depends on the capillary radius according to a power law $Q_{cap} = K_{cap} r_0^{\gamma_{cap}}$, with $(\log(K_{cap}), \gamma_{cap})$ between $(-3.83, 3.30)$ and $(-3.48, 3.19)$, depending on the boundary conditions imposed at the limits of the computational domain[4] (Lorthois et al., 2011a). These values of capillary flow rate as a function of the radius are indicated on Fig. 6 as thin lines, demonstrating that, in the most extreme case (see Fig. 6a, red line), only the largest capillaries can, on average, reach a steady state for tracer exchange because their mean flow is then above $Q_{threshold}$. Even in case of global arterial vasodilations of 25%, *e.g.*, induced by hypercapnia, where the mean capillary flow increases, with $(\log(K_{cap}), \gamma_{cap})$ between $(-3.82, 3.38)$ and $(-3.43, 3.3)$ (unpublished data calculated from Lorthois et al. (2011b), and see Fig. 6, dotted lines), the capillary flow is most often below $Q_{threshold}$.

Note that this conclusion would not be significantly affected by assuming a more realistic input function, *e.g.* a Gaussian bolus. In fact, following the order of magnitude analysis presented above, the lower bound value for the equilibrium flow rate threshold would decrease proportionally to the increase in the duration of the capillary input function due to dispersion. Assuming a dispersion time constant of ~4 s (*e.g.* Meyer, 1989), the total duration of the input function would be ~17 s instead of 13 s. Thus, the lower bound value for the equilibrium flow rate threshold would be ~3/4 of the value predicted with the considered step function. In the log–log plot presented in Fig. 6, this would shift the bold dotted line (transition in case of instantaneous diffusion) toward lower values with a 0.2 decade difference. The same shift or a smaller one is expected in the general case (bold solid line).

In the following, we investigate the ability of the two-compartmental approach to describe the simulated situation.

4.2. Analysis of the reference kinetic data using the Renkin–Crone model

The temporal evolution of the mean concentration in the Krogh cylinder geometry, as determined by numerical simulation, is analyzed using the Renkin–Crone compartmental approach. From Fig. 5 (dashed lines), it can be seen that, for a given geometry (imposed capillary radius) and for each value of the imposed flow rate, the numerical results can in all cases be correctly fitted by Eq. (2). The only adjustable parameter k_1 is determined by minimizing $N(k_1)$ as defined by Eq. (17). From Eq. (19), the permeability coefficient P can then be determined from k_1 if and only if $k_1 v/Q < 1$. Therefore, the results are presented by displaying this last ratio as a function of flow rate in Fig. 7. On the same figure are plotted the asymptotic behaviors expected from Eq. (18): at low flow rate (*i.e.* $Q \ll PS$), $k_1 v/Q$ should reach one (highlighted by the solid line in Fig. 7). This corresponds to the classical *flow-limited* regime usually assumed for interpreting $H_2{}^{15}O$ PET kinetics data, the cerebral blood flow normalized by brain volume (*i.e.* Q/v) being equated with kinetic rate constant k_1. At high flow rate, where $k_1 v/Q \approx PS/Q$ from Eq. (18), a slope-1 (highlighted by the bold segment in Fig. 7) should be reached. This corresponds to a *barrier-limited* regime (*i.e.* $PS \ll Q$), where the kinetic rate constant k_1 loses any relationship to blood flow.

This last asymptotic regime is compatible with the numerical results at high flow rates, *i.e.* a slope approximately −1 can be extracted from the numerical results (see Fig. 7). However, this behavior corresponds to flow rates much higher than mean physiological flows (the order of magnitude of which is spanned by blue and red lines in Fig. 6).

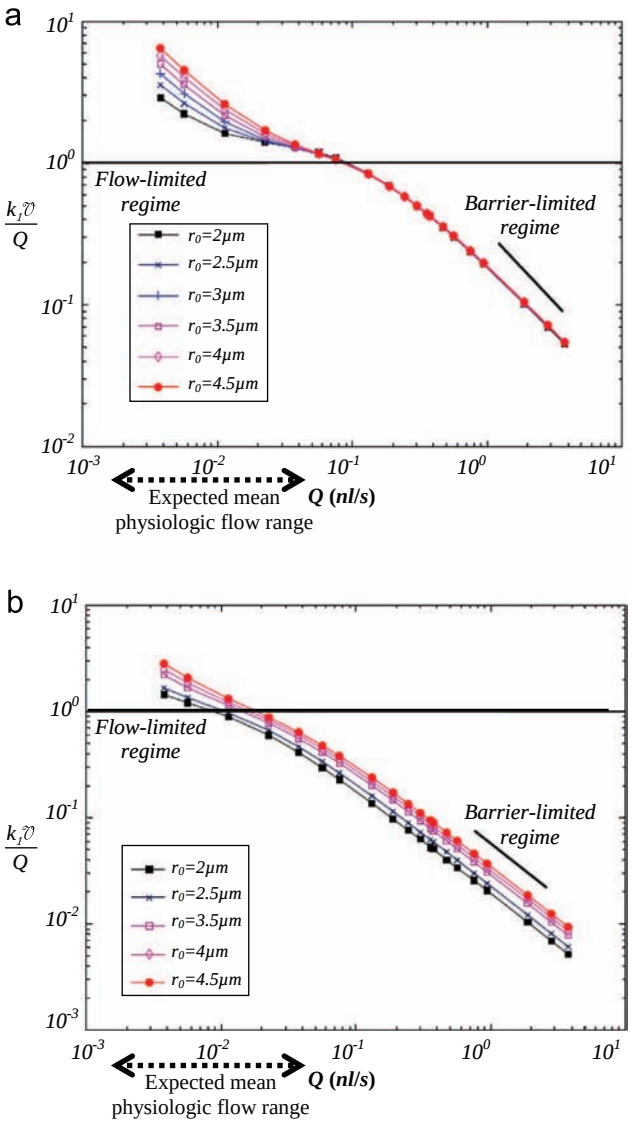

Fig. 7. Renkin–Crone's analysis: parameter $k_1 v/Q$ identified as a function of flow rate for various capillary radii. (a) $D_e = D_t$, $\lambda_d = 1$. (b) $D_e = D_s/100$, $\lambda_d = 0.95$. The thin line ($k_1 v/Q = 1$) corresponds to flow-limited regime. The bold line indicates a slope −1 (barrier-limited asymptotic regime). The bold dotted segment indicates the range of mean physiologic flows in capillary vessels (*i.e.* flow rate range spanned by blue and red lines in Fig. 6).

By contrast, the first asymptotic regime is never reached by the numerical results. The ratio $k_1 v/Q$ is indeed greater than unity for the smallest flow rates. In other words, whatever the flow rate, the value of the restricted water diffusion through the brain capillaries endothelium and the capillary radius are, the *flow-limited* regime is never reached at capillary scale. This result has two consequences. First, the standard assumption that $H_2{}^{15}O$ PET kinetics data can be directly interpreted by assuming a *flow-limited* regime is not valid at capillary scale. Second, at low flow rates, P cannot be determined with the Renkin–Crone approach.

At higher flow rates, Eq. (19) can nevertheless be used to deduce P. Its evolution as a function of flow rate is displayed in Fig. 8. Whatever the value of the restricted diffusion through the endothelial layer, P is found to depend on the flow rate, for the smallest flow rates investigated, and to be highly dependent on the capillary radius, in

[4] In this expression, the capillary radius must be expressed in μm in order to obtain a flow rate expressed in nl/s.

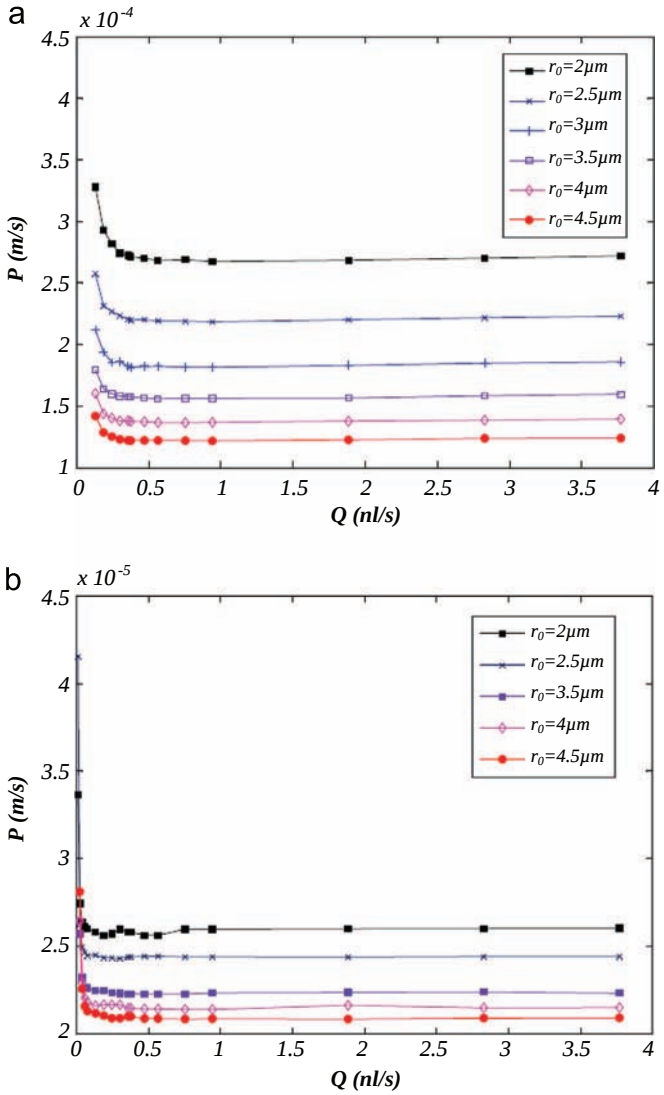

Fig. 8. Renkin–Crone's analysis: permeability coefficient P identified as a function of flow rate for various capillary radii. (a) $D_e=D_t$, $\lambda_d=1$. (b) $D_e=D_s/100$, $\lambda_d=0.95$. Note that when $k_1\nu/Q>1$ (*i.e.* at the lowest flow rates), P remains undetermined.

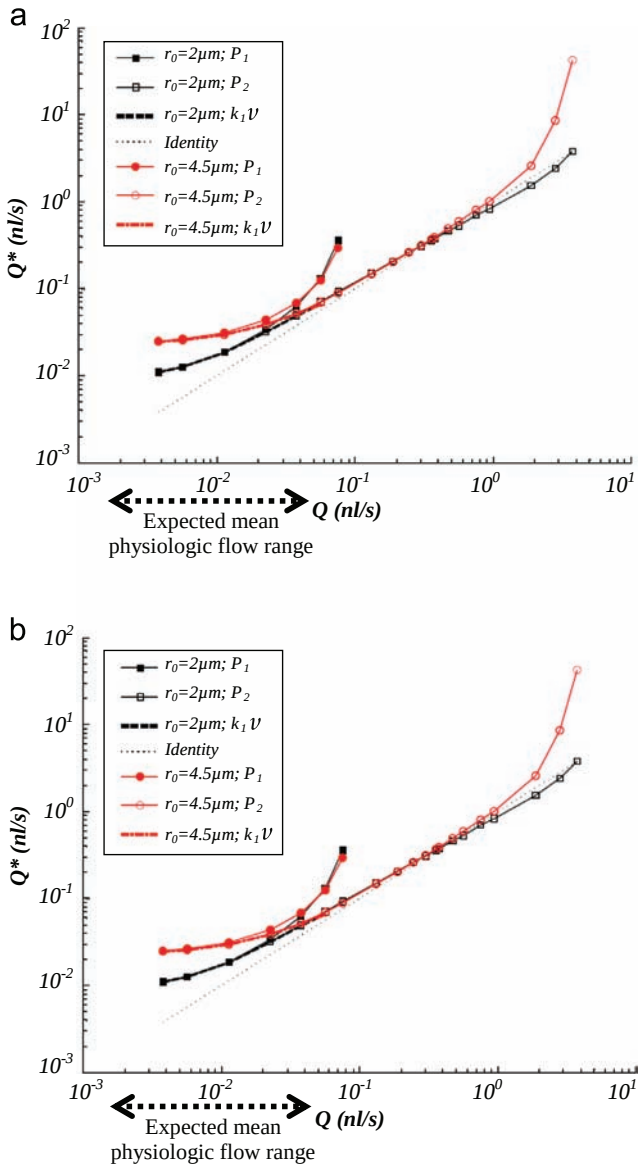

Fig. 9. Renkin–Crone's analysis: flow rate estimated from Eq. (20) as a function of the imposed flow rate for various capillary radii. (a) $D_e=D_t$, $\lambda_d=1$, $P_1=1.218\times10^{-4}$ m/s, $P_2=2.676\times10^{-4}$ m/s; (b) $D_e=D_s/100$, $\lambda_d=0.95$, $P_1=2.085\times10^{-5}$ m/s, $P_2=2.561\times10^{-5}$ m/s. Note that when $PS<k_1\nu$, *i.e.* at high flow rates, Q^* remains undetermined. See inserted legend for details ($k_1\nu$ corresponds to the low flow rate, flow-limited asymptotic regime). Bold dotted segment: same convention as in Fig. 7.

contrast with the central hypothesis of the Renkin–Crone approach, where P is supposed to be a physiological constant.

The dependence of P with r_0 shows that the normalization of the total exchanged flux by the exchange surface (the surface S of the vessel wall) is not sufficient to yield a permeability coefficient independent of the vessel radius. In other words, the exact geometry of the intravascular space influences the exchange process, even at capillary scale.

With these limitations in mind, it is nevertheless possible to study whether the value of the flow rate estimated by using the Renkin–Crone approach is highly sensitive, or not, to the value chosen for P. In order to test this idea, two arbitrary values have been fixed for P, which correspond to the high flow rate asymptotes of the smallest and largest capillary radii considered in this study. In the limit of low flow rates, the choice of P has no influence on the estimated flow rate Q^* (see Fig. 9). This is consistent with the asymptotic behavior of Eq. (20), which predicts that $k_1\nu/Q\sim1$ whatever the value of P (corresponding to the Renkin–Crone *flow-limited* regime). Thus, the predicted flow rate behaves like $k_1\nu$ (dashed-dotted curves). However, as expected because a *flow-limited* regime is never reached at capillary scale (see above), its value does not match the imposed flow rate. In practice, the flow rate is largely over-estimated. By contrast, at high flow rates, the choice of P has a tremendous impact on Q^*. First, in many cases, Q^* cannot be determined (because PS becomes smaller than $k_1\nu$). Second, when Q^* can be determined, it decreases with increasing values of P. Only in one case ($r_0=2$ μm and $P=P_2$), the estimated flow rate closely matches the imposed one over a large range of flow rates.

4.3. Comparison with some PET results

The above results can be compared with classical assumptions used, or results obtained, in the field of cerebral blood flow quantification by $H_2{}^{15}O$ PET, *i.e.* at larger scale.

First, the question whether ^{15}O-labeled water can be considered a freely diffusible tracer is linked to its exchange regime at capillary scale. Our results suggest that, because their flow rate is too small, few capillaries in the brain can reach a steady state for

tracer exchange (equilibrium). Thus, at capillary scale, $H_2{}^{15}O$ is not a freely diffusible tracer. This is consistent with many PET studies demonstrating that ^{15}O-labeled water fails to equilibrate with brain tissue during a single capillary transit, *i.e.* extraction fraction is smaller than one, in human (Herscovitch et al., 1987), monkey (Raichle et al., 1976, Eichling et al., 1974) and rat (Bolwig and Lassen, 1975; Go et al., 1981) brains. Such results highlight the existence of a "*permeability-limitation for water*" (Herscovitch et al., 1987), *i.e.* the permeability coefficient cannot be considered to reach asymptotically high values. As a consequence, the flow rate cannot always be considered to be small compared to the permeability surface product, in contradiction with the classical assumption that PET kinetic data can be analyzed assuming a *flow-limited* regime, where k_1 corresponds to the estimated perfusion by unit volume (Q/v).

Second, the order of magnitude of the permeability coefficients estimated in the present study at capillary scale ($\sim 2\times10^{-5}$ to 30×10^{-5} m/s depending on the diffusion coefficient through the endothelium, see Fig. 8) can be compared with the literature values of the permeability surface product, measured at larger scale in humans (90–170 ml/100 g min, Herscovitch et al., 1987 and references therein). Because we have shown that the exact geometry of the intravascular space influences the exchange process, even at capillary scale, this is probably inappropriate. However, it is interesting because it can give insight into the influence of vascular architecture and/or upscaling process. With the exchange surface of the intra-cortical microvascular network of order $S=5.3$ mm^2/mm^3 (Cassot et al., 2006) and assuming a density of 1.05 for the brain parenchyma (Raichle et al., 1983), yield values from 600 to 9000 ml/(100 g min) for the permeability surface product normalized by brain weight, *i.e.*, much higher than the value measured at brain scale. This suggests that using compartmental models established at capillary scale might lead to incorrect results when analyzing kinetic data acquired at a much larger scale, *i.e.*, voxels in a PET image or larger brain regions of interest.

5. Conclusion: validity of the Renkin–Crone approach at capillary scale

The diffusive transfers between blood and tissue at capillary scale have been studied by numerical simulations. The results have been analyzed using the Renkin–Crone model. The main findings can be summarized as follows:

1. Below a flow threshold $Q_{threshold}$, which is related to the capillary radius by a power law, tracer equilibrium between blood and tissue is *not* reached during tracer injection. Above this threshold, a steady-state equilibrium concentration is reached before rinsing.
2. In both regimes, the tracer kinetics can accurately be fitted by using the Renkin–Crone model. However, for the smallest flow rates, the permeability coefficient cannot be deduced from the adjusted kinetic rate constant, because it then takes imaginary values.
3. At sufficiently large flow rate, the permeability coefficient P deduced from fitting the tracer kinetics by the Renkin–Crone model is highly dependent on flow rate and capillary radius. Therefore, P cannot be considered as a physiological constant, or, in other words, is not conceptually identical to the physiologic capillary permeability.
4. If P is nevertheless considered as a physiological constant, the determination of the flow rate by adjustment of the Renkin–Crone model to the tracer kinetics is very sensitive to the numerical value chosen for this constant, except for low flow rates. However, even for low flow rates, the tracer dynamics at capillary scale does not reach a *flow-limited* regime for the Renkin–Crone approach.

The main flaws of the Renkin–Crone approach lie in the use of the steady state solution for Fick's diffusion across the endothelium and the approximation of the blood and/or tissue regions as well mixed compartments. At the heart of this crude modeling lies the introduction of the permeability coefficient P, which is considered as being a physiological constant. The present results clearly demonstrate that direct numerical simulations data cannot be correctly described within such a framework as P is found in fact to depend on others parameters (flow rate and capillary radius). They are thus consistent with the view of previous authors that "*there is no consensus among the imaging community regarding what measured permeability veritably represents*" (Jennings et al., 2008) and that "*a major limitation of the expression developed by Crone is that the calculation of values of P does not necessarily mean that these values represent actual permeability coefficients…*" (Chinard, 2000).

The computational approach presented here could also be used to study the validity of the more sophisticated models derived from the initial Renkin–Crone analysis (Goresky et al., 1970; Larson et al., 1987; Sawada et al., 1989; Bassingthwaighte et al., 1992; St. Lauwrence and Lee, 1998a,b; Munk et al., 2003a,b). However, because all these models describe the exchange between blood and tissue, at capillary scale, by a single and constant transfer coefficient, the permeability coefficient P, it is likely that none of them will be able to provide a satisfactory framework for analyzing dynamic $H_2{}^{15}O$ PET data in the context of absolute blood flow quantification.

A computational approach similar to that of the present study, although at larger scale, has been presented by Beard and Bassingthwaighte (2000) who solved the convection-diffusion equations in a multi-capillary network. Fitting the simulation data with analytical expressions from a two-compartments distributed model (for which the exchange term between blood and tissue is modeled with an equation similar to Eq. (5)) led to the same kind of inconsistencies as those found in the present study (*e.g.* variation of the best fitting permeability "constant" with flow rate, mismatch between the predicted value of PS and the value expected from physiological measurements). This highlights that such inconsistencies are primarily due to the modeling limitation mentioned above and not to the oversimplifying assumptions regarding the model geometry.

6. Perspectives: upscaling

Finally, while close to physiological reality, the present computational approach has two major limitations. First, it is clearly too sophisticated and costly to be extended to realistic vascular network geometries in brain volumes approaching the size of a PET voxel. Second, it was not designed to be inversed. Thus, it does not provide an operational method allowing the regional cerebral blood flow to be computed from dynamic PET data.

Such an approach is nevertheless useful to understand the dynamic regimes involved in the problem and provide arguments helping to imagine alternative approaches. As suggested by the present results, a major challenge is indeed to progress toward an alternative approach, where the relationship between the transfer coefficient between blood and tissue is explicitly dependent on a series of relevant parameters, which have to be determined. For that purpose, upscaling techniques, such as the volume averaging technique (Quintard and Whitaker, 1995; Whitaker, 1999) can be valuable.

This technique can be used provided some separation of scales exists between the micro-scale and the macro-scale. This is possible in our case because the capillary network is homogeneous

above a cut-off scale (Lorthois and Cassot, 2010). The idea is then to average the fluid dynamic equations written at capillary scale (Eqs. (7)–(9)) in order to obtain the governing equations for the mean concentrations of tracer in tissue and in blood. Such equations feature effective properties, such as effective diffusion coefficients, effective convective transport coefficients and effective mass transfer coefficient between both phases as new parameters. These properties can be numerically calculated as a function of the geometry of the capillary network and of the flow by solving so-called closure problems provided by the theory. This would yield to a generalized macro-scale model (a system of two coupled partial derivative equations representing the spatiotemporal evolution of both mean concentrations in the brain tissue at upscaled scale) with spatially distributed effective properties that could be calculated from tissue scale data. Hence, additional information coming from other investigation techniques, *e.g.*, confocal microscopy (Cassot et al., 2006), vascular-space-occupancy MRI (Lu et al., 2003), *etc*. could be assembled with PET data in a more general and accurate interpretation framework.

Such a mathematical framework for the description in an averaged sense of networks of conductive links embedded in a diffusive material has been developed in other contexts, such as flow in fractured porous media (Quintard and Whitaker, 1996; Ahmadi et al., 1998; Landereau et al., 2001). In particular, it is shown in these papers how to obtain the macro-scale model having the form of a two-equation model, *i.e.*, an advection/diffusion equation for the capillary network coupled through an exchange term with a diffusion equation for the tissues. Such models, like any upscaled models, have some limitations in terms of the response to high frequency input, but the simulations presented in this paper indicates that practical problems of interest are well within their validity domains. In fact, if upscaled models are able to follow the corresponding signal generated by a step function, then lower frequencies, such as those generated throughout the brain tissue, will be accurately represented. Further arguments supporting this encouraging view can be found in Davit et al. (2012).

More specifically, when the geometry of the capillary network is modeled by Krogh's cylinders, the effective mass transfer coefficient mainly depends on two parameters: the mean velocity of capillary blood and the radius of capillaries (Billanou, 2010). This is in agreement with the present results regarding the permeability coefficient and suggests that upscaling techniques could help replacing the compartmental paradigm by a new framework in the context of brain blood flow quantification by PET. Because, contrarily to Eq. (1), both spatial and temporal variables are kept, such a framework would be adapted to describe spatial interactions between voxels. This will allow going beyond the classical approach used for estimating regional cerebral blood flows, where the same arterial input function, only delayed and dispersed, is used for each voxel/region of interest (Walker et al., 2012).

Acknowledgments

We gratefully acknowledge Gérald Debenest for useful discussions. We also thank David Black, Jean-Michel Lagarde, Alexandre Delalleau and Gwendal Josse from the Centre de Recherche sur la Peau for their interest and support.

References

Ametamey, S.M., Honer, M., Schubiger, P.A., 2008. Molecular imaging with PET. Chem. Rev. 108, 1501–1516.

Agre, P., Nielsen, S., Ottersen, O.P., 2004. Towards a molecular understanding of water homeostasis in the brain. Neuroscience 12, 849–859.

Ahmadi, A., Quintard, M., Whitaker, S., 1998. Transport in chemically and mechanically heterogeneous porous media V: two-equation model for solute transport with adsorption. Adv. Water Resour. 22, 59–86.

Amiry-Moghaddam, M., Xue, R., Haug, F.M., Neely, J.D., Bhardwaj, A., Agre, P., Adams, M.E., Froehner, S.C., Mori, S., Ottersen, O.P., 2004. Alpha-syntrophin deletion removes the perivascular but not endothelial pool of aquaporin-4 at the blood–brain barrier and delays the development of brain edema in an experimental model of acute hyponatremia. FASEB J. 18, 542–544.

Bassingthwaighte, J.B., Chan, I.S., Wang, C.Y., 1992. Computationally efficient algorithms for convection–permeation–diffusion models for blood-tissue exchanges. Ann. Biomed. Eng. 20, 687–725.

Beard, D.A., Bassingthwaighte, J.B., 2000. Advection and diffusion of substances in biological tissues with complex vascular networks. Ann. Biomed. Eng. 28, 253–268.

Billanou, I., 2010. Modélisation expérimentale et théorique pour la quantification du débit sanguin par Tomographie à Emission de Positrons (Ph.D. dissertation). INP, Toulouse.

Boulard, G., 2001. Sodium, osmolarité plasmatique et volume cérébral. Ann. Fr. Anest. Réanim. 20, 196–202.

Bourque, C.W., 2008. Central mechanisms of osmosentation and systemic osmoregulation. Nat. Rev. Neurosci. 9, 519–531.

Bolwig, T.G., Lassen, N.A., 1975. The diffusion permeability to water of the rat blood–brain barrier. Acta Physiol. Scand. 93, 415–422.

Coomber, B.L., Stewart, P.A., Hayakawa, K., Farell, C.L., Del Maestro, R.F., 1987. Quantitative morphology of human glioblastoma multiform microvessels: structural basis of blood-brain barrier defect. J. Neuro-oncology 5, 299–307.

Callaghan, P.T., Le Gros, M.A., Pinder, D.N., 1983. The measurement of diffusion using deuterieum pulsed field gradient magnetic nuclear resonance. J. Chem. Phys. 79, 6372–6381.

Cassot, F., Lauwers, F., Fouard, C., Prohaska, S., Lauwers-Cances, V., 2006. A novel three-dimensional computer-assisted method for a quantitative study of microvascular networks of the human cerebral cortex. Microcirculation 13, 1–18.

Chinard, F.P., 2000. Water and solute exchanges. How far have we come in 100 years? What's next?. Ann. Biomed. Eng. 28, 849–859.

Crone, C., 1963. The permeability of capillaries in various organs as determined by use of the “indicator dilution” method. Acta Physiol. Scand. 58, 292–305.

Davit, Y., Wood, B., Debenest, G., Quintard, M., 2012. Correspondence between one- and two-equation models for solute transport in two-region heterogeneous porous media. Transp. Porous Media 95, 213–238.

Dolman, D., Drndarski, S., Abbott, N.J., Rattray, M., 2005. Induction of aquaporin 1 but not aquaporin 4 messenger RNA in rat primary brain microvessel endothelial cells in culture. J. Neurochem. 93, 825–833.

Eichling, J.O., Raichle, M.E., Grubb, R.L., Ter-Pogossian, M.M., 1974. Evidence of the limitations of water as a freely diffusible tracer in brain of the rhesus monkey. Circ. Res. 35, 358–364.

Fenstermacher, J., Kaye, T., 1988. Drug “diffusion” within the brain. Ann. NY Acad. Sci. 531, 29–39.

Fraser, P.A., Dallas, A.D., 1990. Measurement of filtration coefficient in single cerebral microvessels of the frog. J. Physiol. 423, 343–361.

Golfier, F., Quintard, M., Cherblanc, F., Zinn, B.A., Wood, B.D., 2007. Comparison of theory and experiment for solute transport in highly heterogeneous porous medium. Adv. Water Resour. 30, 2235–2261.

Goresky, C.A., Ziegler, W.H., Bach, G.G., 1970. Capillary exchange modeling. Barrier-limited and flow-limited distribution. Circ. Res. 27, 739–764.

Go, G.K., Lammerstsma, A.A., Paans, A.M.J., Vaalburg, W., Woldring, M.G., 1981. Extraction of water labeled with oxygen 15 during single capillary transit. Influence of blood pressure, osmolarity and blood–brain barrier damage. Arch. Neurol. 38, 581–584.

Hawkins, B.T., Davis, T.P., 2005. The blood–brain barrier/neurovascular unit in health and disease. Pharmacol. Rev. 57, 173–185.

Herscovitch, P., Raichle, M., 1985. What is the correct value for the brain–blood partition coefficient for water? J. Cereb. Blood Flow Metab. 5, 65–69.

Herscovitch, P., Raichle, M.E., Kilbourn, M.R., Welch, M., 1987. Positron emission tomographic measurement of cerebral blood flow and permeability-surface area product of water using ^{15}O-water and ^{11}C-butanol. J. Cereb. Blood Flow Metab. 7, 527–542.

Heymann, J.B., Engel, A., 1999. Aquaporins: phylogeny, structure, and physiology of water channels. News Physiol. Sci. 14, 187–193.

Innis, R.B., Cunningham, V.J., Delforge, J., Fujita, M., Gjedde, A., Gunn, R.N., Holden, J., Houle, S., Huang, S.C., Ichise, M., Iida, H., Ito, H., Kimura, Y., Koeppe, R.A., Knudsen, G. M., Knuuti, J., Lammertsma, A.A., Laruelle, M., Logan, J., Maguire, R.P., Mintun, M.A., Morris, E.D., Parsey, R., Price, J.C., Slifstein, M., Sossi, V., Suhara, T., Votaw, J.R., Wong, D.F., et Carson, R.E., 2007. Consensus nomenclature for *in vivo* imaging of reversibly binding radioligands. J. Cereb. Blood Flow Metab. 27, 1533–1539.

Jennings, D., Raghunand, N., Gillies, R., 2008. Imaging hemodynamics. Cancer Metastasis Rev. 27, 589–693.

Kety, S.S., Schmidt, C.F., 1948. The nitrous oxide method for the quantitative determination of cerebral blood flow in man: theory, procedure and normal values. J. Clin. Invest. 27, 476–483.

Kety, S.S., 1951. The theory and applications of the exchange of inert gas at the lungs and tissues. Pharmacol. Rev. 3, 1–41.

Krogh, A., 1919. The number and distribution of capillaries in muscles with calculations of the oxygen pressure head necessary for supplying the tissue. J. Physiol. 52, 409–415.

Kimelberg, H.K., 2004. Water homeostasis in the brain: basic concepts. Neuroscience 129, 851–860.
Kuschinsky, W., Paulson, O.B., 1992. Capillary circulation in the brain. Cerebrovasc. Brain Metab. Rev. 4, 261–286.
Landereau, P., Noetinger, B., Quintard, M., 2001. Quasi-steady two-equation models for diffusive transport in fractured porous media: large-scale properties for densely fractured systems. Adv. Water Resour. 24, 863–876.
Larson, K.B., Markham, J., Raichle, M.E., 1987. Tracer-kinetic models for measuring cerebral blood flow using externally detected radiotracers. J. Cereb. Blood Flow Metab. 7, 443–463.
Lauwers, F., Cassot, F., Lauwers-Vance, V., Puwanarajah, P., Duvernoy, H., 2008. Morphometry of the human cerebral cortex microcirculation: general characteristics and space-related profiles. Neuroimage 39, 936–948.
Lassen, N.A., Perl, W., 1979. Tracer kinetic methods in medical physiology. Raven Press, New York.
Li, G., Yuan, W., Fu, B.M., 2010. A model for the blood–brain barrier permeability to water and small solutes. J. Biomech. 43, 2133–2140.
Lorthois, S., Cassot, F., 2010. Fractal analysis of vascular networks: insights from morphogenesis. J. Theor. Biol. 262, 614–633.
Lorthois, S., Cassot, F., Lauwers, F., 2011a. Simulation study of brain blood flow regulation by intra-cortical arterioles in an anatomically accurate large human vascular network: Part I: methodology and baseline flow. Neuroimage 54, 1031–1042.
Lorthois, S., Cassot, F., Lauwers, F., 2011b. Simulation study of brain blood flow regulation by intra-cortical arterioles in an anatomically accurate large human vascular network: Part II: flow variations induced by global or localized modifications of arteriolar diameters. Neuroimage 54, 2840–2853.
Lu, H., Golay, X., Pekar, J.J., van Zijl, P.C.M., 2003. Functional magnetic resonance imaging based on changes in vascular space occupancy. Magnetic Resonance in Medicine 50, 263–274.
Maallem, S., Mutin, M., Kwon, H.M., Tappaz, M.L., 2006. Differential cellular distribution of tonicity-induced expression of transcription factor TonEBP in the rat brain following prolonged systemic hypertonicity. Neuroscience 137, 51–71.
MacAulay, N., Hamann, S., Zeuthen, T., 2004. Water transport in the brain: role of cotransporters. Neuroscience 129, 1031–1044.
Meyer, E., 1989. Simultaneous correction for tracer arrival delay and dispersion in CBF measurements by the H2150 autoradiographic method and dynamic PET. J. Nucl. Med. 30, 1069–1078.
Michel, C.C., Curry, F.E., 1999. Microvascular permeability. Physiol. Rev. 79, 703–761.
Morris, E.D., Endres, C., Schmidt, K., Christian, B., Muzic, R.F., Fisher, R., 2004. Kinetic modeling in PET. In: Wernick, M., Aarsvold, J. (Eds.), Emission Tomography: The Fundamentals of PET and SPECT. Academic Press, San Diego (chapter 23).
Munk, O.L., Bass, L., Feng, H., Keiding, S., 2003a. Determination of regional flow by use of intravascular pet tracers: microvascular theory and experimental validation for pig livers. J. Nucl. Med. 44, 1862–1870.
Munk, O.L., Keiding, S., Bass, L., 2003b. Capillaries within compartments: microvascular interpretation of dynamic positron emission tomography data. J. Theor. Biol. 225, 127–141.
Nicholson, C., 2001. Diffusion and related transport mechanisms in brain tissue. Rep. Prog. Phys. 64, 815–884.
Papahadjopulos, D., Kimelberg, H.K., 1974. Phospholipid vesicles (liposomes) as models for biological membranes: their properties and interactions with cholesterol and proteins. Progress in Surface Science 5, 141–232.
Pardrige, W.M., 2002. Drug and gene delivery to the brain: the vascular route. Neuron 36, 555–558.
Paulson, O.B., Hertz, M.M., Bolwig, T.G., Lassen, N.A., 1977. Filtration and diffusion of water across the blood–brain barrier in man. Microvac. Res. 13, 113–123.
Paulson, O.B., 2002. Blood–brain barrier, brain metabolism and cerebral blood flow. Eur. Neurophychopharmacol. 12, 495–501.
Pawlik, G., Rackl, A., Bing, R.J., 1981. Quantitative capillary topography and blood flow in the cerebral cortex of cats: an *in vivo* microscopic study. Brain Res. 208, 35–58.
Quarles, R.P., Mintum, M.A., Larson, K.B., Markham, J., McLeod, A.M., Raichle, M.E., 1993. Measurement of regional cerebral blood flow with positron emission tomography: a comparison of [^{15}O] water to [^{11}C] butanol with distributed-parameter and compartmental models. J. Cereb. Blood Flow Metab. 13, 733–747.
Quintard, M., Whitaker, S., 1995. Local thermal equilibrium for transient heat conduction: theory and comparison with numerical experiments. Int. J. Heat Mass Transf. 38, 2779–2796.
Quintard, M., Whitaker, S., 1996. Transport in chemically and mechanically heterogeneous porous media I: theoretical development of region averaged equations for slightly compressible single-phase flow. Adv. Water Resour. 19, 29–47.
Raichle, M.E., Eichling, J.O., Straatmann, M.G., Welch, M.J., Larson, K.B., Ter-Pogossian, M.M., 1976. Blood–brain barrier permeability of ^{11}C-labeled alcohols and ^{15}O-labeled water. Am. J. Physiol. 230, 543–552.
Raichle, M.E., Martin, W.R.W., Herscovitch, P., Mintun, M.A., Markham, J., 1983. Brain blood flow measured with intravenous $H_2{}^{15}O$. II. Implementation and validation. J. Nucl. Med. 24, 790–798.
Renkin, E.M., 1955. Effects of blood flow on diffusion kinetics in isolated, perfused hindlegs of cats: a double circulation hypothesis. Am. J. Physiol. 183, 125–136.
Renkin, E.M., 1959. Transport of potassium-42 from blood to tissue in isolated mammalian skeletal muscles. Am. J. Physiol. 197, 1205–1210.
Rudakova, M., Filippov, A., Skirda, V., 2004. Water diffusivity in model biological membranes. Appl. Magn. Reson. 27, 519–526.
Sawada, Y., Patlak, C.S., Blasberg, R.G., 1989. Kinetic analysis of cerebrovascular transport based on indicator diffusion technique. Am. J. Physiol. Heart Circ. Physiol. 256, H794–H818.
St. Lauwrence, K., Lee, T., 1998a. An adiabatic approximation to the tissue homogeneity model for water exchange in the brain: I theoretical derivation. J. Cereb. Blood Flow Metab. 18, 1365–1377.
St. Lauwrence, K., Lee, T., 1998b. An adiabatic approximation to the tissue homogeneity model for water exchange in the brain: II experimental validation. J. Cereb. Blood Flow Metab. 18, 1378–1385.
Stanisz, G.J., Li, J.G., Wright, G.A., Henkelman, R.M., 1998. Water dynamics in human blood via combined measurements of T2 relaxation and diffusion in the presence of gadolinium. Magn. Reson. Med. 39, 222–233.
Taylor, R., Krishna, R., 1993. Multicomponent Mass Transfer. John Wiley & Sons, New York.
Thomas, D.L., Lythgoe, M.F., Pell, G.S., Calamante, F., Ordidge, R.J., 2000. The measurement of diffusion and perfusion in biological systems using magnetic resonance imaging. Phys. Med. Biol. 45, R97–R138.
Villringer, A., Them, A., Lindauer, U., Einhaüpl, K., Dirnagl, U., 1994. Capillary perfusion of the rat brain cortex: an *in vivo* confocal microscopy study. Circ. Res. 75, 55–62.
Walker, M.D., Feldmann, M., Matthews, J.C., Anton-Rodriguez, J.M., Wang, S., Koepp, M.J., Asselin, M.D., 2012. Optimiztion of methods for quantification of rCBF using high-resolution [^{15}O]H_2O PET images. Phys. Med. Biol. 57, 2251–2271.
Weisstein, E.W., 2002. CRC Concise Encyclopedia of Mathematics, 2nd edition CRC Press.
Whitaker, S., 1999. The method of volume averaging. Kluwer Academic Publishers, Dordrecht.